

UNCERTAINTIES IN THE SIMULATION OF BED EVOLUTION IN RECIRCULATING FLOW AREA BEHIND GROYNES*

M. YASI

Dept. of Water Engineering, Urmia University, Urmia, I. R. of Iran
Email: m.yasi@yahoo.com

Abstract– The main characteristic of the flow induced by groynes is the development of a recirculating flow area. An interaction between the recirculating flow and bed mobility leads to the development of a scour hole around the groyne, and a sediment deposition bar downstream. The simulation of the bed evolution around a groyne was investigated by linking a developed sediment transport model (STM-2D) to the FAST-2D flow model. The flow model was modified for the present study to simulate the detailed characteristics of the flow around the groyne. The previous study by the author indicated that the results of the numerical simulations compare well with the experimental data in two cases of the flows in flat-bed channels and in channels with complex-bed topography induced by a groyne.

The present state of sediment transport relationships, in particular the relationships for calculating the bed-shear stress and the bed-load transport rate, was evaluated as an essential step for the computational simulation of the groynes performance. A depth-averaged version of the bed-shear stress relationship was modified with the inclusion of correction factors for the effects of the local spiral motion and of the local bed topography. Sediment transport relationships of Ackers and White, and of van Rijn (both deterministic and stochastic methods) were adapted. A number of difficulties were encountered in the development and validation of this model, nevertheless, substantial progress was made. This paper discusses the major uncertainties in the simulation process. It is concluded that modification of the conventional bed-shear stress relationship is not sufficient for simulating realistically the bed features behind the groyne. The development of a conceptual method for calculating the bed-shear stresses around groynes is a priority and recommended for future studies.

Keywords– River modeling, groynes, recirculating flow, bed-shear stress, bed load, bed evolution

1. INTRODUCTION

In river engineering practice, groynes are widely used for such purposes as river training, stream bank protection, and rectifying navigable rivers [1]. Groynes are generally oriented transverse to the flow direction, extending from the bank into the channel. They provide indirect protection by diverting potentially erosive currents away from the stream bank and by guiding the flow in a desired channel course. The main function of the groynes is to reduce the current along the streambank, thereby inducing the deposition of the sediment downstream and between neighbouring groynes [1, 2].

Few experiments appear to have been conducted to investigate the overall bed configuration, including the scoured area and the deposition of the sediment behind the groyne [1, 3]. A detailed experimental study was carried out by Yasi [2] to illustrate the bed deformation and its relationship to the characteristics of recirculating flow induced by a single groyne in a straight, sand-bed channel. This information is considered to be an essential pre-requisite for the numerical modeling of groynes.

*Received by the editors September 21, 2004; final revised form October 3, 2005.

The literature indicates that the application of the numerical models for simulating the flow pattern around the groynes is still limited. The most well-known flow models with groynes are: the modified TEACH-2D model [4]; FAST-2D model [5, 6]; the 2D model of Molls and Chaudhry [7]; and the CCHE-3D model [8, 9]. Except for the FAST-2D model, all have been tested against data in flat, fixed-bed channels with a single groyne. Using a similar data set, major improvements were not evident from the predictions of the 3D model, CCHE, when compared with those of the 2D models [2]. In addition, the 3D model could not properly simulate the velocity gradient in the vertical direction near the groyne, resulting from the non-hydrostatic pressure distribution in this area [2]. A FAST-2D model was tested with the data from a large-scale physical model of the Rhine river with groynes present [10, 11]. This model has been tested with the data from a large-scale physical model of an 11.1 km reach of the river Rhine in Germany with a series of groynes present. The results indicate that this model is capable of simulating the flows in rivers with irregular boundaries and with hydraulic structures such as bridge piers and groynes. However, the detailed recirculating flow in the groyne field was not evaluated in the model. The FAST-2D model is consistent with that of Tingsanchali and Maheswaran [4] in employing the governing equations, but is considered to be superior because of the efficient numerical scheme for simulating the flows in a complex, natural river geometry.

Numerical models for simulating the temporal variation of the bed behind groynes are very limited. Zaghoul and McCorquodale [12] and Blondeaux and Colombini [13] simulated only the scour around the toe of a single groyne in a straight channel. However detailed results on the computed flow field and bed deformation were neither presented nor experimentally verified [12, 13]. Przedwojski's 2D numerical model [14] does not describe the impact of groynes on flow recirculation and the redistribution of bed sediment around and within the groyne field.

The prediction of the temporal development of the bed topography behind groynes is considered to be a complex process to model numerically. An interaction between recirculating flow and the bed mobility behind the groyne leads to subsequent changes in the flow, sediment transport, and bed topography. This feedback process is complex, in particular in its developing stages. For this reason, numerical models have not yet been advanced sufficiently to simulate the bed evolution behind groynes. However, mathematical modeling could be possible by linking a water- flow model to an appropriate sediment- transport model. The proper simulation requires a stepped procedure as: 1) Providing an appropriate flow model applicable to rivers with complex bed geometry and irregular boundaries; 2) Verifying the model for the proper reproduction of the recirculating flow behind the groyne in fixed-bed channels; 3) Testing the flow model against detailed data in a movable-bed channel with the groyne present; 4) Evaluating the reproduction of bed-shear stresses around the groyne; 5) Developing an appropriate sediment transport model for simulating bed evolution in conjunction with the flow model.

In the present study, the 2D, steady- flow model (FAST-2D) [5, 6] was modified by Yasi [2] to enhance the simulation of flow around groynes. Detailed characteristics of the recirculating flows were reproduced by the modified FAST-2D model around a groyne in a straight channel. The results of the numerical calculations compared well with experimental data for two study cases in fixed-bed conditions: 1) on smooth-flat bed channels; and 2) on sand-bed channels with complex-bed topography induced by the groyne at the equilibrium state of the bed [2].

A sediment transport model (STM-2D) was developed for use in conjunction with the modified FAST-2D flow model in order to test the present state of sediment transport relationships in a straight channel with the groyne present [2]. The performance of the numerical model was tested against the flow situation and bed deformation in movable-bed experiments. This paper addresses major uncertainties in achieving the goal of computational simulation of the bed geometry behind groynes, in particular the scour around the groyne and the deposition of sediment downstream.

2. MATERIALS AND METHODS

a) Flow model

The simulation of the flow pattern behind groynes was examined using a two-dimensional (depth-averaged), steady flow model (FAST-2D) developed at the Institute for Hydromechanics, University of Karlsruhe, Germany. Details of the governing equations and the model are presented by Wenka [5] and Zhu [6]. In a curvilinear system, the complete set of equations is written in the common tensor form as

$$\frac{\partial}{\partial x_i} (C_i \phi + D_{i\phi}) = J S_\phi \quad ; i = 1, 2 \tag{1}$$

The dependent variable ϕ represents a depth-averaged physical quantity, leading to the expression of Eq. (1) in the form of 5 conservation equations as presented in Table 1. For each of the variables ϕ , the term C_i relates to convection and $D_{i\phi}$ relates to diffusion, and these are separately presented in Table 1. The source term S_ϕ in the momentum equations includes the pressure gradient ($\partial p / \partial x_i$) and the components of the bed-shear stresses, $\tau_{b,i}$.

Table 1. Extension of Eq. (1) in the FAST-2D flow model [14, 19]

Equation	ϕ	C_i ($i = 1, 2$)	$D_{i\phi}$ ($i = 1$)	$D_{i\phi}$ ($i = 2$)	S_ϕ
Continuity	1	$h c_i$	0	0	0
Momentum in x-direction	V_1	$h c_i$	$-\frac{v_i}{J} h (D_1 + \beta_1^1 \omega_1^1 + \beta_2^1 \omega_1^2)$	$-\frac{v_i}{J} h (D_2 + \beta_1^2 \omega_1^1 + \beta_2^2 \omega_1^2)$	$\frac{1}{\rho} \tau_{b,1} - \frac{h}{\rho J} \left[\frac{\partial}{\partial x_1} (P\beta_1^1) + \frac{\partial}{\partial x_2} (P\beta_1^2) \right]$
Momentum in y-direction	V_2	$h c_i$	$-\frac{v_i}{J} h (D_1 + \beta_1^1 \omega_2^1 + \beta_2^1 \omega_2^2)$	$-\frac{v_i}{J} h (D_2 + \beta_1^2 \omega_2^1 + \beta_2^2 \omega_2^2)$	$\frac{1}{\rho} \tau_{b,2} - \frac{h}{\rho J} \left[\frac{\partial}{\partial x_1} (P\beta_2^1) + \frac{\partial}{\partial x_2} (P\beta_2^2) \right]$
Turbulence- Kinetic Energy	k	$h c_i$	$-\frac{v_i}{\sigma_k} \frac{h}{J} (D_1)$	$-\frac{v_i}{\sigma_k} \frac{h}{J} (D_2)$	$\frac{1}{C_j} \frac{U_*^3}{h} + \frac{1}{\rho} G - \epsilon$
Dissipation Rate	ϵ	$h c_i$	$-\frac{v_i}{\sigma_\epsilon} \frac{h}{J} (D_1)$	$-\frac{v_i}{\sigma_\epsilon} \frac{h}{J} (D_2)$	$C_{cr} \frac{C_{2s}}{C_j^{3/4}} C_\mu^{1/2} \frac{U_*^4}{h^2} + C_{1\epsilon} \frac{\epsilon}{k} \left(\frac{1}{\rho} G \right) - C_{2\epsilon} \frac{\epsilon^2}{k}$

$\beta_j^i = \text{cofactor of } \partial y_j / \partial x_i \text{ in } J$
 $B_j^i = \beta_1^i \beta_1^j + \beta_2^i \beta_2^j, \quad \omega_j^i = \beta_j^1 \frac{\partial V_1}{\partial x_1} + \beta_j^2 \frac{\partial V_1}{\partial x_2}, \quad J = \begin{vmatrix} \frac{\partial y_1}{\partial x_1} & \frac{\partial y_2}{\partial x_1} \\ \frac{\partial y_1}{\partial x_2} & \frac{\partial y_2}{\partial x_2} \end{vmatrix}$
 $v_i = C_\mu k^2 / \epsilon$
 $G = \frac{\mu_t}{J^2} \left\{ 2(\beta_1^1 \frac{\partial V_1}{\partial x_1} + \beta_2^1 \frac{\partial V_1}{\partial x_2})^2 + 2(\beta_1^2 \frac{\partial V_2}{\partial x_1} + \beta_2^2 \frac{\partial V_2}{\partial x_2})^2 + (\beta_1^2 \frac{\partial V_1}{\partial x_1} + \beta_2^2 \frac{\partial V_1}{\partial x_2} + \beta_1^1 \frac{\partial V_2}{\partial x_1} + \beta_2^1 \frac{\partial V_2}{\partial x_2})^2 \right\}$

$c_1 = (V_1 \beta_1^1 + V_2 \beta_2^1), \quad c_2 = (V_1 \beta_1^2 + V_2 \beta_2^2)$
 $D_1 = B_1^1 \frac{\partial \phi}{\partial x_1} + B_2^1 \frac{\partial \phi}{\partial x_2}, \quad D_2 = B_1^2 \frac{\partial \phi}{\partial x_1} + B_2^2 \frac{\partial \phi}{\partial x_2}$
 $C_\mu = 0.09, C_{1\epsilon} = 1.44, C_{2\epsilon} = 1.92, \sigma_k = 1.0, \sigma_\epsilon = 1.3$
 $\sigma_{cr} = 1.8 \quad : (\text{natural river flow})$
 $\sigma_{cr} = 3.6 \quad : (\text{ideal flow})$

The FAST-2D model uses an efficient finite-volume method with boundary-fitted curvilinear grids, and an iterative process to solve the governing equations of continuity and momentum. Horizontal turbulence transport is simulated with the standard depth-averaged version of k-ε turbulence model. This numerical feature, however, requires an additional pressure-velocity coupling scheme to solve momentum equations by an iterative procedure. The pressure-velocity coupling is achieved with the SIMPLEC algorithm in which the momentum equations are initially solved with a prescribed distribution of water depths, subsequently corrected during an internal iteration process. The numerical scheme uses Cartesian velocity components and HYBRID central / upwind differencing for discretization. The resulting system of linear equations is solved with the Thomas tridiagonal matrix algorithm via the iteration procedure until the prescribed convergence is achieved [6].

This model was originally tested by Yasi [2] against the flow situations observed in the fixed-bed experiments with the groyne. It was concluded that the efficiency of the model depends largely on the modification of the k- ε turbulence model, bed-shear stresses, proper adoption of physical and numerical boundary conditions, and the resolution of the numerical grid around the groyne. A proper simulation of the recirculating flow area was considered to be the most significant determinant in evaluating the flow model. Subsequently, the original k- ε model was modified with the inclusion of correction factors for the effects of the turbulent spiral motion and streamline curvature. This correction modifies the dissipation term ($C_2\varepsilon^2/k$) of the source term of the ε -equation in Table 1 in the following form:

$$C_2 \frac{\varepsilon^2}{k} (1 - C_c R_{it}) \quad (2)$$

where $k=0.4$ is the von Karman constant; R_{it} = the turbulent Richardson number [4]; and $(1 - C_c R_{it}) = CCKE$ is the curvature correction term for the k- ε model. The calibration coefficient C_c was introduced for the effect of the groyne length in a simple form of $C_c = 3b - 0.2$ (where b is the groyne length). This modification produced close simulations of the recirculating flow characteristics, in particular the geometry of the separation zone observed in fixed-bed tests [11].

The depth-averaged bed shear stress relationship [15] was modified with the inclusion of correction factors for the effects of the local spiral motion and bed topography in the following form [2, 14].

$$\tau_b = C_f \rho (U^2 + V^2) \{ [K_b] [1 + K_s^2]^{1/2} \} \quad (3)$$

where τ_b = bed shear stress; U and V are the depth-averaged values of the x- and y- velocity components; C_f = the shear coefficient; ρ = the water density; K_b = the bed factor; and K_s = the correction factor due to the spiral motion.

The shear coefficient C_f is determined differently depending on the relative roughness of the bed. For rough surfaces, the Manning equation is used with the convenience of choosing the Manning roughness coefficient, n , as follows:

$$C_f = \frac{gn^2}{h^{1/3}} \quad (4)$$

in which h = local water depth and g = acceleration due to gravity.

Equations for K_b and K_s have been adapted through personal communication between the author and Przedwojski [16] by the following relationships.

$$K_b = \left[1 + \left(\frac{\partial Z_b}{\partial x} \right)^2 + \left(\frac{v}{u} \right)^2 \left(\frac{\partial Z_b}{\partial y} \right)^2 + 2 \frac{v}{u} \left(\frac{\partial Z_b}{\partial x} \right) \left(\frac{\partial Z_b}{\partial y} \right) \right]^{1/2} \quad (5)$$

$$K_s = C_c Ah \left(\frac{1}{R_s} \right) \quad (6)$$

in which A = the weighting coefficient for the influence of spiral motion and R_s = the local radius of streamline curvature, as expressed by

$$A = \frac{2}{k^2} \left[1 - \frac{\sqrt{C_f}}{k} \right] \quad \text{and} \quad \frac{1}{R_s} = \frac{uv \left(\frac{\partial v}{\partial y} - \frac{\partial u}{\partial x} \right) + u^2 \frac{\partial v}{\partial x} - v^2 \frac{\partial u}{\partial y}}{(u^2 + v^2)^{3/2}} \quad (7)$$

The modified FAST-2D model was calibrated with two experimental data in a flat, fixed-bed channel. Subsequently, the application of the model was verified in two movable-bed experiments against the equilibrium bed topography induced by the groyne in a sand-bed channel. The comparative results indicated that the distributions of water depths and velocities are satisfactorily reproduced. The reproduction of bed-shear stresses (τ_b) in the movable-bed channel was, however, uncertain because of the lack of specific experimental data. Specific conclusions for the adequacy of Eq. (3) in predicting the bed-shear stresses around the groyne are presented in the following sections.

b) Sediment transport model

Bathymetric variations are governed by the continuity equation of sediment transport, for which the formulation for the magnitude and direction of the sediment transport rate must be included. In the present study, bed-load transport is considered to be significant in the bed evolution. Using the Cartesian coordinate system, the 2D sediment continuity equation for straight channels [2] is expressed as:

$$\frac{\partial Z_b}{\partial t} + \frac{1}{(1-\lambda)} \left(\frac{\partial q_{bx}}{\partial x} + \frac{\partial q_{by}}{\partial y} \right) = 0 \quad (8)$$

where Z_b = the local bed elevation; $\partial Z_b / \partial t$ = the change in the local-bed level during the time interval ∂t ; λ = the porosity of the bed material; and q_{bx} and q_{by} = the x- and y- components of the bed-load transport q_b per unit width, respectively.

The components of the bed-load transport are expressed in terms of the direction angle of sediment transport relative to the x-axis (α) by

$$q_{bx} = q_b \cos \alpha \quad ; \quad q_{by} = q_b \sin \alpha \quad (9)$$

Among the existing sediment transport formulae, the relationships of Ackers and White [17], and van Rijn [18] are well adapted to the experimental conditions in the present study. The inclusion of the criterion for the initiation of sediment motion in these relationships has the major advantage of distinguishing the regions where the bed shear stress exceeds the critical value for the bed material.

The sediment transport rate in the method of Ackers and White [17] is expressed as follows:

$$q_t = \frac{G_{gr} D_{35}}{h} \left(\frac{U}{U_*} \right)^n q \quad (10)$$

in which q_t = the total volumetric sediment transport rate per unit width ($m^3/s/m$); G_{gr} = the sediment transport function; D_{35} = the size for which 35% of the bed material is finer (m); h = the water depth (m); U = the mean flow velocity (m/s); q = the flow rate per unit width ($m^3/s/m$); and U_* = the shear velocity (m/s). Although the bed-load transport is not directly calculated from the Ackers and White relationships, the basic theory and calculation processes are strongly related to bed-shear stresses and the properties of bed sediment. It is considered that the bed-load transport could be calculated by this method under upstream clear-water flows, or with a degree of over-estimation.

Van Rijn [18] presented two different approaches (i.e., Deterministic and Stochastic) for calculating the bed-load transport. In the deterministic approach, the bed-load transport is related to the mean values of bed-shear stresses as follows:

$$q_b = 0.053 \sqrt{g(S_g - 1)} D_{50}^{1.5} \frac{T_s^{2.1}}{D_{gr}^{0.3}} \quad \text{if } T_s < 3 \quad (11)$$

$$q_b = 0.10 \sqrt{g(S_g - 1)} D_{50}^{1.5} \frac{T_s^{1.5}}{D_{gr}^{0.3}} \quad \text{if } T_s \geq 3 \quad (12)$$

in which q_b = the volumetric bed-load transport rate per unit width ($\text{m}^3/\text{s}/\text{m}$); $T_s = (\tau_b - \tau_c)/\tau_c$ = the transport stage parameter; D_{gr} = the dimensionless characteristic particle parameter; S_g = the specific gravity (dimensionless); D_{50} = the size for which 50% of the bed material is finer (m); τ_b = the effective bed-shear stress (N/m^2); τ_c = the critical bed-shear stress (N/m^2).

In the stochastic approach, van Rijn [18] assumed that the instantaneous bed-load transport rate is related to the instantaneous transport parameter T_s as follows:

$$q_b = C_b (\sqrt{g(S_g - 1)} \frac{D_{50}^{1.5}}{D_{gr}^{0.3}}) \bar{T}_s^{2.1} \quad (13)$$

where C_b is a coefficient ranging from 0.053 to 0.1; and $\bar{T}_s^{2.1}$ is the time-averaged shear stress parameter which is expressed as:

$$\bar{T}_s^{2.1} = E[T_s^{2.1} | \tau_b \geq \tau_{c1}] - E[T_s^{2.1} | \tau_b \leq \tau_{c2}] \quad (14)$$

in which E signifies the expected value, and τ_{c1} and τ_{c2} are the instantaneous critical bed-shear stress along the flow direction and against the flow direction, respectively.

The direction of sediment transport, α , in Eq. (9) is calculated with the relation of Koch and Flokstra [19] as follows:

$$\tan \alpha = \frac{\tau_b \sin \delta - S_p \frac{\partial Z_b}{\partial y}}{\tau_b \cos \delta - S_p \frac{\partial Z_b}{\partial x}} \quad \text{where} \quad S_p = \frac{2}{3} [\rho g (S_g - 1)] \frac{D_{50}}{f_s \lambda_b} \quad (15)$$

in which S_p represents the characteristics of the bed material, f_s = the shape factor of the sediment particles, λ_b = the sheltering coefficient for the effects of the resistance force due to the friction and keying between neighboring particles, Z_b = the local bed elevation; and δ = the direction of bed-shear stress relative to the x - axis. The effects of the main flow direction and local spiral motion are included in the calculation of δ using the following relationship:

$$\delta = \arctan\left(\frac{V}{U}\right) - \arctan\left(Ah \left(\frac{1}{R_s}\right)\right) \quad (16)$$

in which h = the local water depth, A = the weighting coefficient for the influence of spiral motion (Eq. 7), and R_s = the local radius of streamline curvature (Eq. 7).

The governing equations for sediment transport are numerically solved in the conservative form using the finite-volume method, similar to that in the flow model. Using the Cartesian coordinates system, Eq. (8) is discretized for a control volume in the following difference form:

$$\left(\frac{\Delta Z_b}{\Delta t}\right)_p \approx -\left(\frac{1}{1 - \lambda}\right) \left[\frac{(q_{bx})_e - (q_{bx})_w}{x_e - x_w} + \frac{(q_{by})_n - (q_{by})_s}{y_n - y_s} \right] \quad (17)$$

where ΔZ_b is the averaged-bed elevation centered at the control volume, and the subscripts e , w , n , and s represent the east-, west-, north-, and south- faces of the control volume.

A computer program (STM-2D) was developed to numerically solve the sediment continuity (Eq. 17) for a given flow condition and a prescribed bed topography in straight channels (Fig. 1).

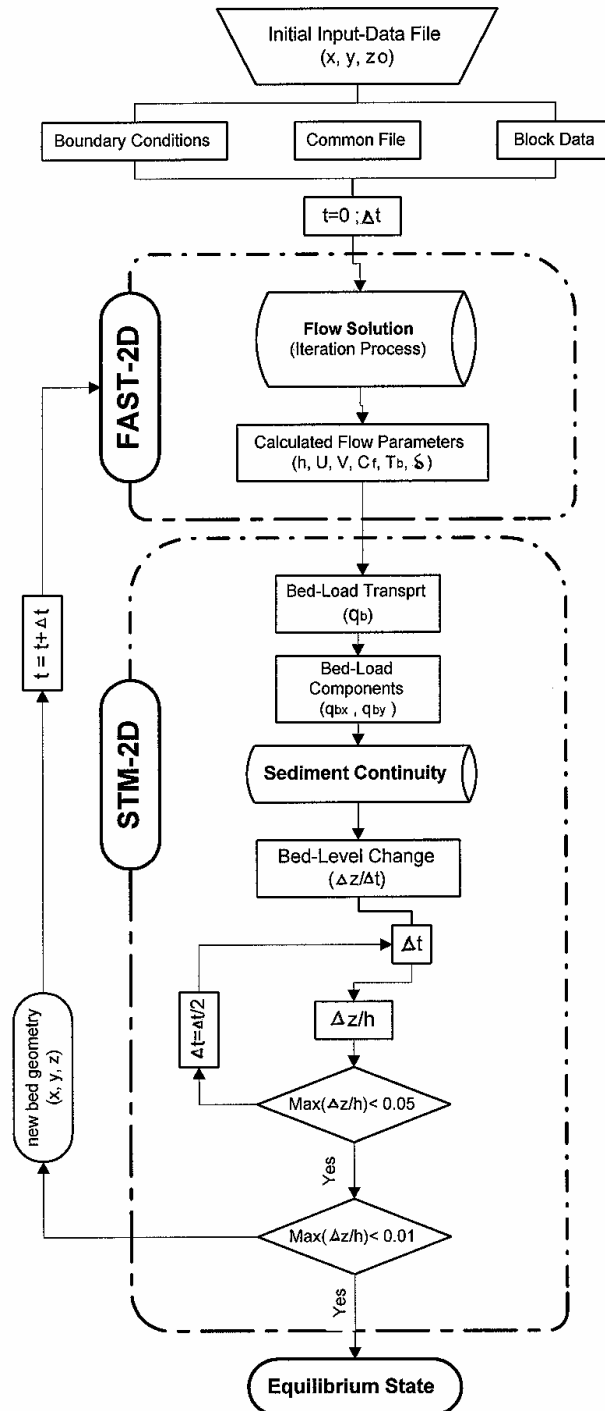


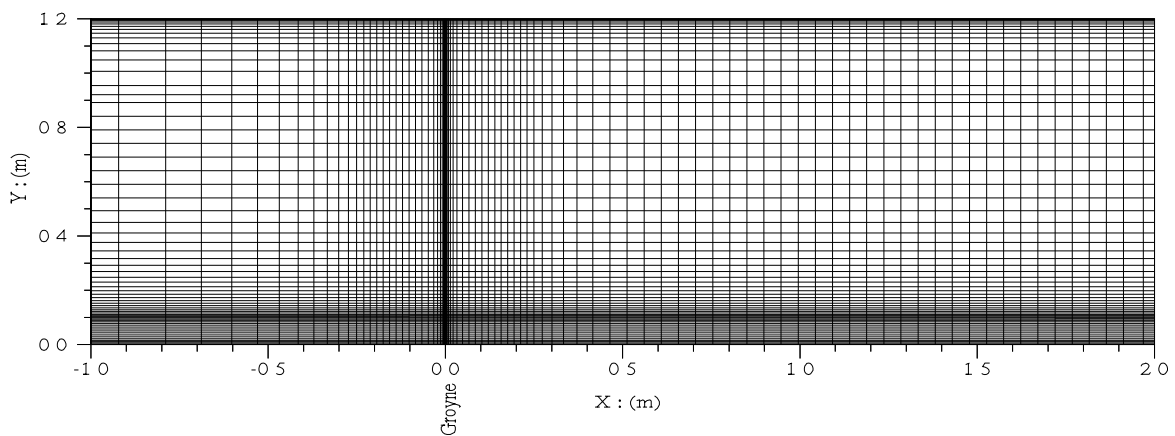
Fig. 1. Flow chart for simulating bed evolution

c) Solution procedure

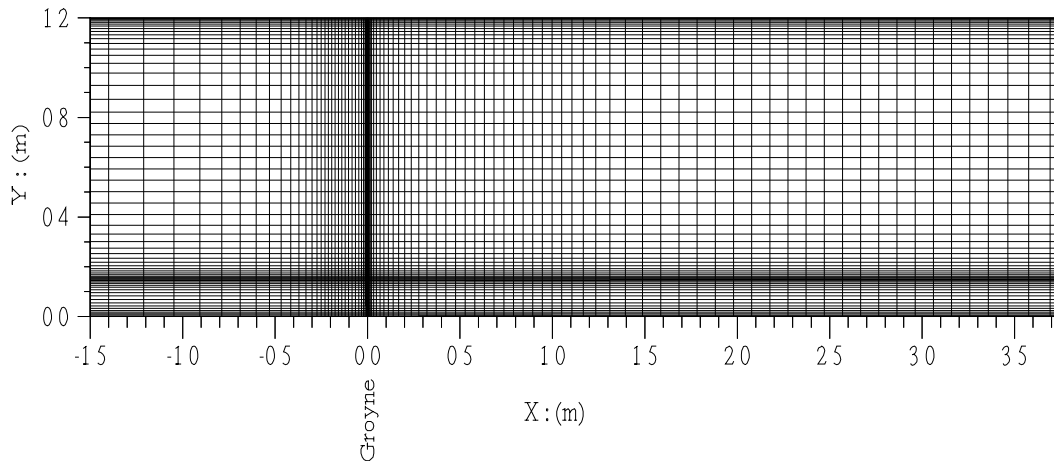
An uncoupled approach was taken to simulate the flow and bed evolution. In this procedure, the modified steady flow model (FAST-2D) is linked to the unsteady sediment transport model (STM-2D) for an interactive solution between the flow parameters and bed variations. This approach is known as "Quasi-steady flow modeling". It is considered that the bed-level variation with respect to time is very small when

compared with the corresponding change in the water depth. Therefore, the flow and bed evolution can be treated separately in each time step, during which the bed is kept unchanged for the flow calculations. Bed load (q_b) is evaluated at the beginning of each time step using the flow parameters and bed geometry calculated from the previous time step. An equilibrium condition is always reached by a numerical computation marching forward in time over a sufficiently long period.

The overall structure of the numerical simulation of the bed evolution and the sequence of computational processes are illustrated in Fig. 1. Boundary-fitted grid size, such as that presented in Fig. 2, is considered for stable and converged solution. The iterative procedure is repeated to the eventual equilibrium state of the bed, when the rate of the bed-level changes ($\Delta Z_b/\Delta t$) is negligible. As seen in Fig. 1, it is assumed that the equilibrium state is reached when the calculated maximum bed-level change is 1% of the corresponding local water depth or the maximum bed-level change is less than D_{90} of the bed material over the flow field, whichever is greater [2].



a) Grid Size (88×65) in Test M1, (groyne length, $b=0.1$ m located at $X=0.0$ m, on RHS)



b) Grid Size (94×62) in Test M2, (groyne length, $b=0.15$ m located at $X=0.0$ m, on RHS)

Fig. 2. Computational grid in the movable-bed tests M1 and M2

d) Experiments

An experimental study was conducted in a straight, rectangular channel with a length of 12 m, a width of 1.2m, and a depth of 0.5m with smooth-glassed bed and sides. The bed level was relocated 260 mm above the glass bed allowing for the placement of the bed material. The bed material was a quartz-based

sand, with the specific gravity of $S_g = 2.65$. The grain size ranged from 1.0 to 2.4 mm, with the median diameter, $D_{50} = 1.7$ mm. The critical bed shear stress was estimated for the sand to be $\tau_c = 1.02$ N/m². The groyne comprised a rectangular-sheet metal plate 3mm thick and 0.5m high in length 100 and 150 mm. The test reach was located in the middle of the channel and had a length of 7 m, starting 2.5 m from the upstream end. The groyne was placed 4.0 m from the upstream end of the channel, projecting perpendicular to the flow field.

The desired flow condition required a channel slope of $S = 0.05\%$, and a flow rate of $Q = 36$ l/s. The approach flow was subcritical and fully-turbulent rough flow. The bed-shear stress in the approach flow, τ_{bo} , was 0.342 N/m². Therefore, the ratio of τ_{bo} / τ_c was less than unity denoting upstream clear-water conditions. Table 2 presents the general conditions under which two experiments M1 and M2 were carried out.

Table 2. Physical and flow conditions in the movable-bed experiments with groynes

Test	B (m)	b (m)	α	θ (°)	Q (m ³ /s)	h (m)	U (m/s)	Fr	Re ($\times 10^{-6}$)	τ_{bo} (N/m ²)	τ_{bo} / τ_c
M 1	1.20	0.10	0.92	90	0.036	0.11	0.27	0.26	1.5	0.34	0.34
M 2	1.20	0.15	0.88	90	0.036	0.10	0.29	0.28	1.6	0.32	0.31

* Bed material : Sand ; $D_{50} = 1.7$ mm ; $S_g = 2.65$; $\tau_c = 1.02$ N/m² (Critical bed-shear stress)
 B = Channel width ; b = Groyne length ; Q = Flow rate ; h = Water depth; U = Mean velocity;
 Fr = Froude No. ; Re = Reynolds No. ; τ_{bo} = Upstream bed-shear stress.

During the long period of the experiment, the process of interaction between the flow and the bed was initiated by an interference mechanism between the groyne and the approach flow in the movable-bed channel. In developing stages, the main feature of the bed was developed around the groyne. This feature was generally similar in the two tests M1 and M2. Figure 3 shows the bathymetry 24 hours following the commencement of the test M1. Contours of negative values indicate the scouring area relative to the initial bed level, while positive ones show the extent of deposition.

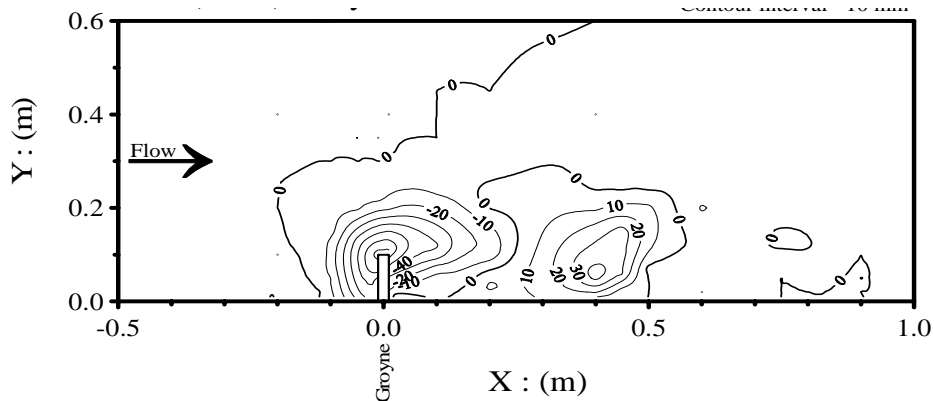
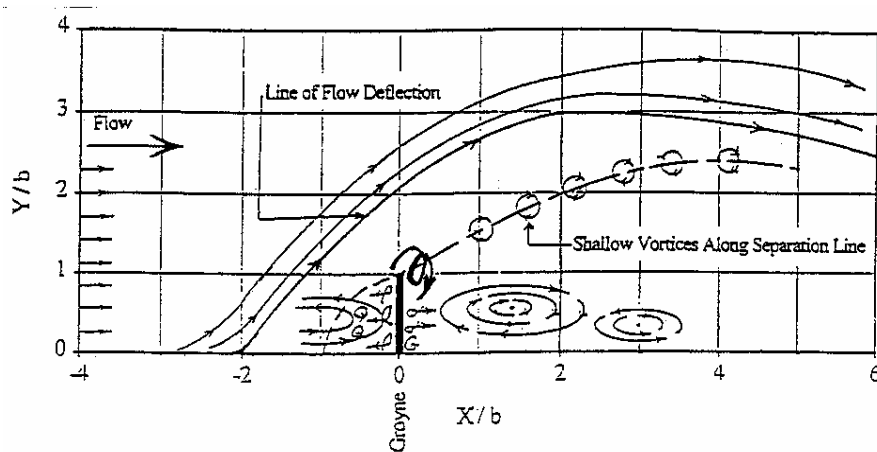
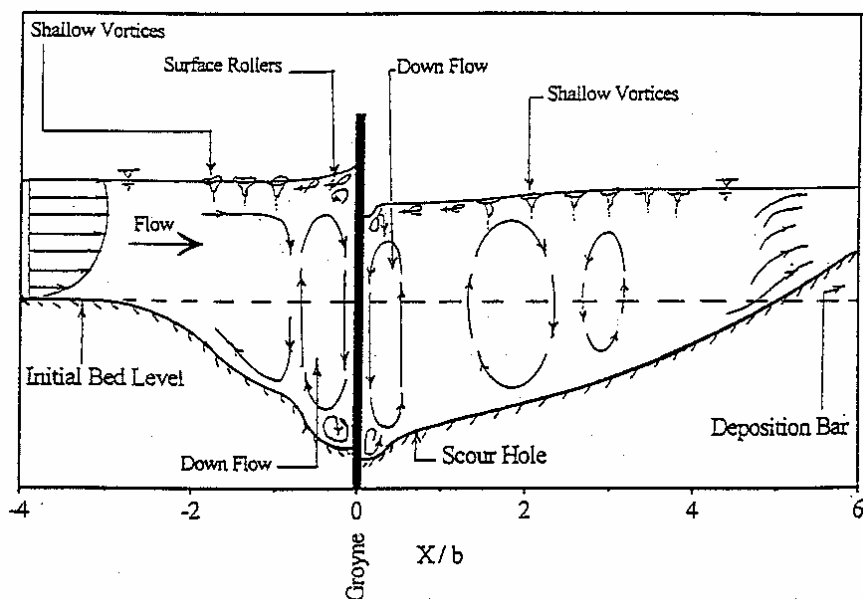


Fig. 3. Observed bed evolution behind the groyne in Test M1

Velocity vectors were measured over the flow depth around the groyne. From the observation and the measured velocity vectors, Fig. 4 shows, schematically, the system of vortices associated with the flow and the extent of the scour hole around the groyne and deposition area downstream. Details of the experimental design and procedure, and the results on the structure of the recirculating flow and bed geometry behind the groyne are presented elsewhere by Yasi [2].



a) Plan view of flow pattern near water surface



b) Cross-sectional profile near the tip of the groyne

Fig. 4. A schematic view of flow pattern and system of vortices around the groyne

e) Model application

In the numerical modelling, the channel bed was initially considered to be flat with a constant longitudinal slope of 0.5%. This condition was consistent with that of the beginning of the movable-bed experiments. A distance of $10b$ and $20b$ from the groyne (b = groyne length) was sufficient for the upstream and downstream boundaries of the flow field, respectively [2]. Based on the geometry of the flume and the groyne structure, the grid system was characterised as a boundary-fitted, non-uniform, structured, orthogonal grid in the (x - y) plane. A smooth transition was considered in the longitudinal and lateral grid spacings (near the walls and the structure) based on the law of the wall [2]. Initial computations were carried out to optimise the grid size based on the stability of the converged solution and the number of iterations. The best arrangement resulted in a grid size of (88×65) for Test M1, and of (94×62) for Test M2, as presented in Fig. 2. Uniform flow was introduced beyond the upstream and downstream boundaries. The initial and boundary conditions were specified at the inlet, outlet, and rigid walls. The plan form of the groyne was considered as a blocked-off region into the flow field. Therefore, the boundary conditions of the rigid walls were implemented on each side of the groyne.

The modified FAST-2D flow model was first tested for the cases of flow in flat-bed channels and in channels with complex-bed geometry, with the groyne present [2]. Both results were sufficiently good. These two cases are considered to represent a reliable application of the flow model at different stages of the bed evolution, starting from an initial flat bed towards a deformed bed configuration induced by the groyne.

Computations began with the prescribed flat bed and proceeded in time to determine the transient development of the bed, as illustrated in Fig. 1. For the flow calculations with the FAST-2D model, for test M1, the solution converged with 264 iterations at each time step. For the sediment transport module, an initial time interval Δt was set to 100 sec. This time increment could be refined automatically to achieve a convergence criterion of a maximum of 5.5 mm change in the bed level in each time step. The equilibrium state of the bed was checked at subsequent time steps, until when the maximum bed-level change become less than $D_{90} = 2.2$ mm.

3. RESULTS AND DISCUSSION

a) Computational results

Calculation of flow parameters with the FAST-2D model is independent of those of bed variations with STM-2D at each time step. For this reason, the reproduction of bed deformation behind the groyne is considered to be appropriate for evaluating the components of the STM-2D model, when compared with that in the experiment. The predictive capability of the model depends, to a great extent, on the relationships for calculating bed-shear stresses, τ_b , and sediment transport rate q_s . Consequently, the development of the bed was evaluated by: 1) The application of the bed-shear stress relationship with and without the modification for the effects of the local spiral motion and bed geometry; 2) The application of the total-load relationship of Ackers and White, and bed-load formulae of van Rijn (both deterministic and stochastic methods). With respect to the present targets, the results and general conclusions from the computed- bed configuration were similar in the two tests M1 and M2. Hence, the following sections focus on the typical results from the test M1.

b) Bed-shear stress relationships

For the first time step at which the channel bed is flat, the calculated τ_b is considered to be the most important determinant of the bed material motion around the groyne. The bed-shear stresses, τ_b , were calculated in the program using Eq. (3), initially without the modification for the effects of the local spiral motion and bed geometry (i.e., $K_s = 0$ and $K_b = 1$ in Eq. 3), and then with modification for these effects.

Without modification of Eq. (3), a detailed contour map of calculated τ_b is presented in Fig. 5 at the initial stage of the bed ($t = 0$), for a distance range of $4 \leq X/b \leq 12$ and $Y/b \leq 4$ around the groyne, in test M1. At the upstream section, the average value of τ_b was calculated to be 0.31 N/m^2 , which is close to $\tau_{b0} = 0.34 \text{ N/m}^2$ in the test M1. The critical bed-shear stress was $\tau_c = 1.02 \text{ N/m}^2$ for the bed material. Hence, the ratio of τ_{b0}/τ_c is less than unity in the approach flow, implying clear-water flow upstream the groyne. Figure 5 also indicates that the ratio of (τ_b/τ_{b0}) increases by about 50% at the toe of the groyne and in the deflected flow area downstream, in a distance range of $0 \leq X/b \leq 10$ and $1 < Y/b \leq 4$. Figure 5 shows that the bed shear stress does everywhere calculated to be less than the critical value for the bed material (i.e., $\tau_b/\tau_c < 1$), leading to zero bed-load transport ($q_b = 0$) and no bed change. Hence, the program stopped after the first time step. This result was independent of the choice of the bed-load relationships. Furthermore, the calculated values of τ_b were very small within the recirculating flow area compared to those upstream. It is considered that the bed-shear stresses corresponding to the depth-averaged velocities are not competent to initiate bed motion around the groyne at the early stage of the bed evolution.

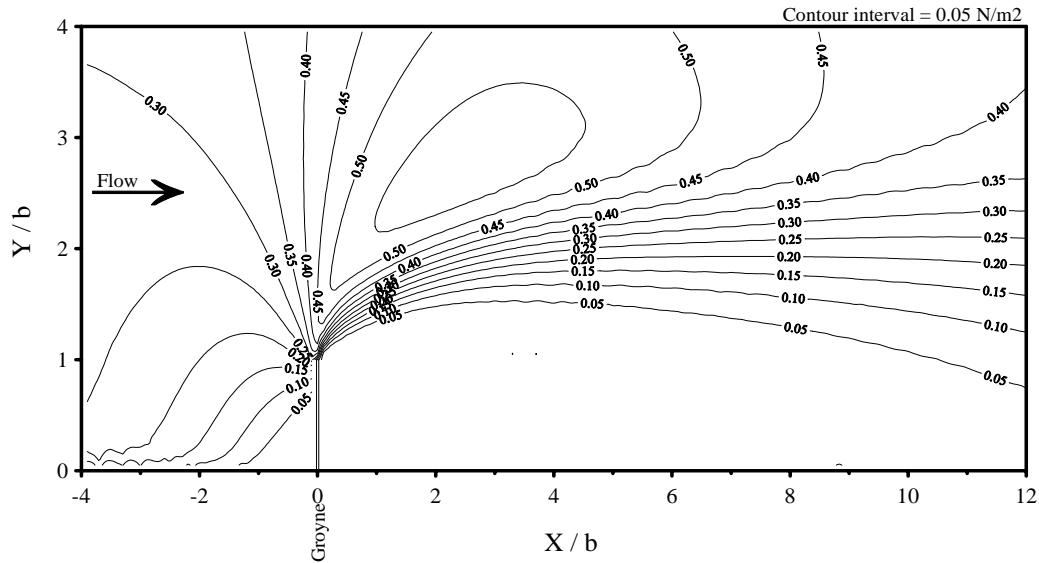


Fig. 5. Contour map of bed-shear stresses at the initial stage (Test M1), without correction factors K_b and K_s in Eq. (3)

The bed-shear stress field calculated with the modified bed-shear stress relationship (Eq. (3)) is presented in Fig. 6, at the initial stage of the bed. Comparative plots between Figs. 5 and 6 indicate a significant magnification in the calculated τ_b within a distance range of $-1.5 < X/b < 1$ and $Y/b < 2$, which is consistent with the main scoured area in the movable-bed experiment M1. Near the toe of the groyne, the maximum bed-shear stress increased from 0.58 N/m^2 for the unmodified Eq. (3), to 2.3 N/m^2 as a result of the high velocity gradients and strong flow curvatures in this area. Since the ratio of τ_b/τ_c is significantly greater than the one around the groyne nose, the bed level evolves with time. Different bed-load relationships were used for subsequent time steps, in order to evaluate the bed deformation.

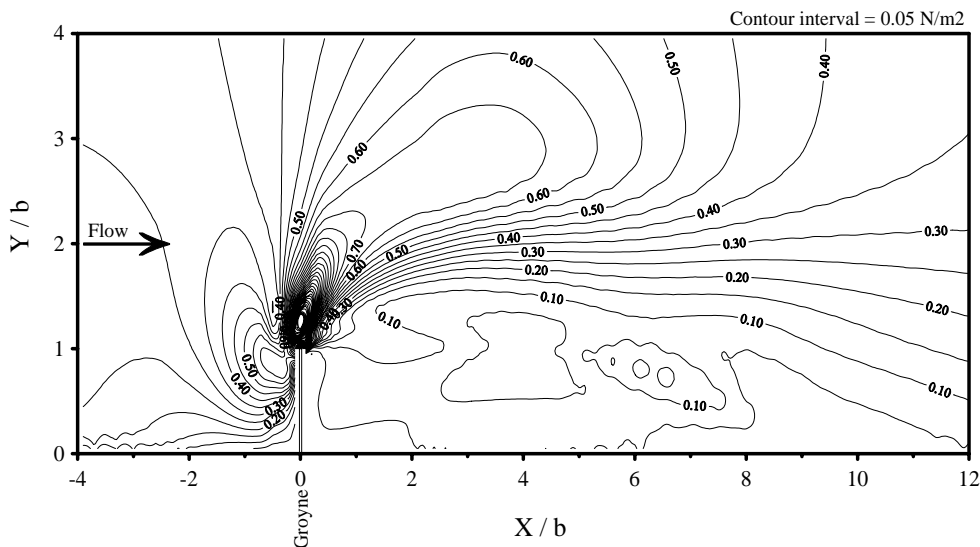


Fig. 6. Contour map of bed-shear stresses at the initial stage (Test M1), with correction factors K_b and K_s in Eq. (3)

c) Bed-load relationships

The sediment transport relationship of Ackers and White (Eq. (10)) was found to be inappropriate for simulating the bed variations around the groyne. The computed sediment transport was zero everywhere in the flow field, leading to no bed change around the groyne and the program stopped running. This condition occurred even at the groyne nose, where a significant increase in τ_b existed. It was concluded

that the Ackers and White relationship is more dominated by the depth-averaged velocity than the bed-shear stress, and that the mean velocities within the recirculating flow area are very small.

Both the deterministic and stochastic bed-load relationships of van Rijn (Eqs. (11-14)) were found to be sufficiently responsive to the local variation of τ_b/τ_c around the groyne, producing significant bed-level variations in subsequent time steps. The computed bathymetry was similar for the two methods. Figures 7 and 8 present the bed deformation using the deterministic and stochastic relationships, respectively, for the same development time as that in Fig. 3, in the test M1. In these figures, contours of negative values indicate the scouring area relative to the initial zero bed level, while positive values show the extent of the deposition of the eroded bed material. The scoured area is located at the front of the groyne nose on the upstream and downstream face of the groyne, whereas the eroded material is deposited downstream of the scoured area. However, the comparison between Fig. 7 or 8 and Fig. 3 shows poor agreement.

In the computational process, the scour depth grew up to 125 mm (after 120 and 200 time steps using the deterministic and stochastic methods, respectively) at the groyne nose ($X/b = -0.1$ and $Y/b = 1.1$). This was consistent with the location and magnitude of the maximum scour depth observed in the experiment M1 [2], but the bed level was continuing to change in subsequent time steps in the computational process. Furthermore, as shown in Fig. 7 or 8, the bed variation was restricted to an area between $-0.5 < X/b < 0.5$ and $0.5 < Y/b < 2$, and did not significantly vary during sequent time steps, whereas the bed level varied continuously with time within this area. Significant changes occurred to the bed level within a distance range of $-1.5 < X/b < 1$ and $Y/b < 2$, which is identical to that of the magnified τ_b in Fig. 6. It was noticed that the calculated values of τ_b did not sufficiently reduce to the threshold value of τ_c during the developing stages of the bed scour around the groyne. Consequently, the prescribed equilibrium condition for the bed was not satisfied.

The comparison between Figs. 7 and 8 shows that the application of the stochastic method of van Rijn did not improve the simulated process when compared with the deterministic method. Considering the uncertainties in determining the statistical parameters, the application of the stochastic method would not be superior to the deterministic method at this stage.

It is evident that the modification imposed in the form of Eq. (3), although magnifying the bed-shear stresses sufficiently to produce sediment motion, is insufficient for reproducing a realistic distribution of the bed-shear stresses in flows with the groyne present. The discrepancy between the observed and calculated bed topography around the groyne is primarily related to the proper prediction of bed-shear stresses in the recirculating flow area around the groyne. The efficiency of the bed-load relationships of van Rijn is dominated by the functioning of the bed-shear stresses, and is considered to be of second priority in this process.

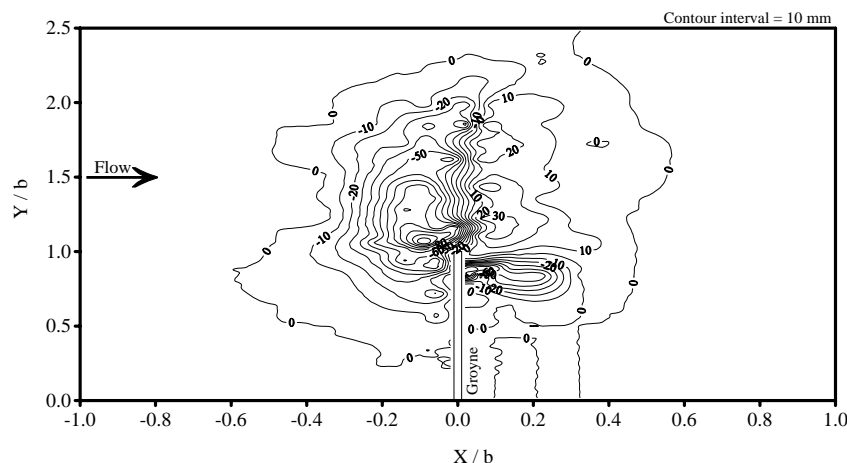


Fig. 7. Contour map of simulated bed deformation around the groyne in Test M1 (using deterministic method of van Rijn)

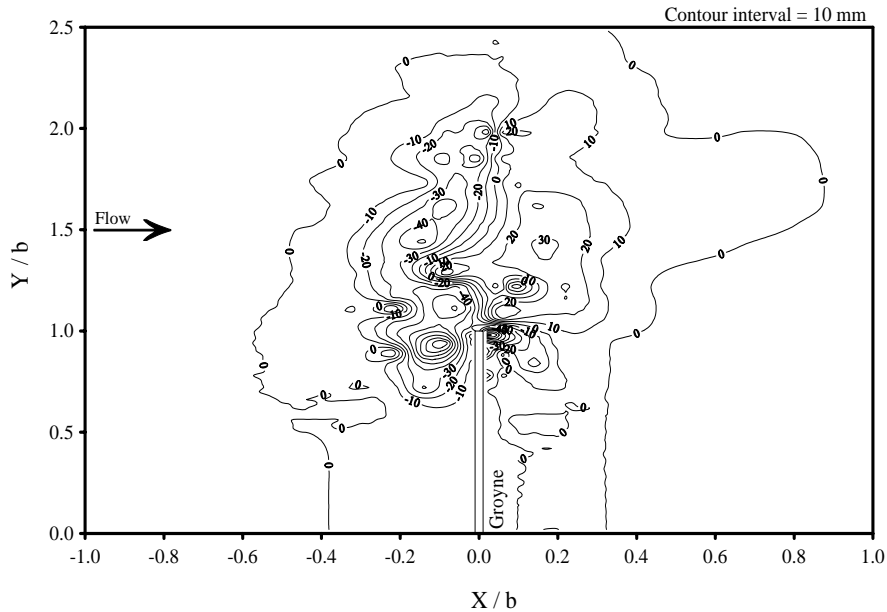


Fig. 8. Contour map of simulated bed deformation around the groyne in Test M1 (using stochastic method of van Rijn)

4. CONCLUSIONS

The prediction of time-dependent bed topography behind groynes is an important objective in numerical modeling. The simulation process was investigated by linking the two models (FAST-2D and STM-2D) for an interactive solution between the flow parameters and bed variations right to the eventual dynamic equilibrium state of the bed, as illustrated in Fig. 1. The predictive efficiency of the model was found to depend, to a great extent, on the relationships for calculating bed-shear stresses and sediment transport rate in the groyne- induced field.

It is concluded that the mean velocities are not sufficient alone for calculating τ_b in the recirculating flows with the groyne present. The inclusion of correction factors for the effects of the local spiral motion (K_s) and of the local bed topography (K_b) in the form of Eq. (3) imposes a significant modification in the calculated τ_b around the groyne within a distance range of $-1.5 < X/b < 1$ and $Y/b < 2$. Consequent significant bed variations occur around the groyne within an area between $-0.5 < X/b < 0.5$ and $0.5 < Y/b < 2$ when either the deterministic or the stochastic bed-load relationships of van Rijn [13] was tested. Beyond this region, the distribution of τ_b is not competent to reproduce the bed variations.

It is also concluded that the calculated values of τ_b do not sufficiently reduce to the threshold value of τ_c during the developing stages of the bed scour around the groyne; consequently the prescribed equilibrium condition of the bed is not achieved. Moreover, the aerial extent of the bed variations (i.e. scour and deposition) does not progress well with time. The application of the stochastic method was not superior to the deterministic method in the simulation process. The simulated bed topography is considered to be unrealistic when compared with that observed in two movable-bed experiments.

It is evident that the proper formulation of bed-shear stresses in the recirculating flow area around the groyne- like structures is the first priority. Because of the specific mechanism of the local scour process, it is concluded that the effect of generated downward currents, vortices, and turbulence intensity must be included in the bed-shear stress relationship. The development of such a conceptual method is necessary to improve the sediment transport model. Detailed measurement of the turbulent fluctuation of bed-shear stresses is essential within an area between $-4 \leq X/b \leq 12$ and $0 \leq Y/b \leq 4$ around the groyne for the validation of such a relationship. The efficiency of the bed-load relationships of van Rijn is dominated by

the functioning of the bed-shear stress relationship, and is considered to be of second priority in this process. The development of a concrete coupled model for the simultaneous solution of unsteady flow and sediment governing equations is an eventual objective which has to be acknowledged.

REFERENCES

1. Copeland, R. R. (1983). Bank protection techniques using spur dikes. *Hydraulics Laboratory, U.S. Army Corps of Engineers, Waterways Experiment Station, Vicksburg, Mississippi.*
2. Yasi, M. (1997). Flow and bed geometry behind a groyne. Ph D Thesis, Department of Civil Engineering, Monash University, Melbourne, Australia.
3. Suzuki, K., Michiue, M. & Hinokidani, O. (1987). Local bed form around a series of spur-dikes in alluvial channels. *Proceedings, 22nd Congress IAHR, Lausanne, 316-321.*
4. Tingsanchali, T. & Maheswaran, S. (1990). 2-D depth-averaged flow computation near groyne. *Journal of Hydraulic Engineering, ASCE, 116(1) 71-86.*
5. Wenka, Th. (1992). Numerische berechnung von stromungsvorgangen in naturnahen flublaufen mit einem tiefengemittelten modell. Ph.D. Thesis, Institute for Hydromechanics, the University of Karlsruhe, Germany, in German.
6. Zhu, J. (1991). FAST-2D: A computer program for numerical simulation of two-dimensional incompressible flows with complex boundaries. Report No. 690, Institute for Hydromechanics, the University of Karlsruhe, Germany.
7. Molls, T. & Chaudhry, M. H. (1995). Depth-averaged open-channel flow model. *Journal of Hydraulic Engineering, ASCE, 121(6) 453-465.*
8. Jia, Y. & Wang, S. S. Y. (1993). 3D numerical simulation of flow near a spur dike. *Advances in Hydro-Science and -Engineering, (1) 2150-2155.*
9. Mayerle, R., Toro, F. M. & Wang, S. S. Y. (1995). Verification of a three-dimensional numerical model simulation of the flow in the vicinity of spur dikes. *Journal of Hydraulic Research, IAHR, 33(2) 243-256.*
10. Wenka, T., Rodi, W. & Nestmann, F. (1993). Depth-averaged calculation of flow in river reaches with flood control and sediment regulation structures. *Proceedings, 25th Congress IAHR, Tokyo, Japan.*
11. Wenka, Th., Valenta, P. & Rodi, W. (1991). Depth-averaged calculation of flood flow in a river with irregular geometry. *Proceedings, 24th Congress, IAHR, Madrid, Spain.*
12. Zaghoul, N. & McCorquodale, J. (1973). A numerical model for flow past a spur-dike. *Proceedings, First Canadian Hydraulics Conference, Canada, (1) 355-68.*
13. Blondeaux, P. & Colombini, M. (1987). A model for scour around spur-dikes. *Proceedings, 22nd Congress IAHR, Section A: Fluvial Hydraulics, Lausanne, 311-315.*
14. Przedwojski, B. (1995). Bed topography and local scour in rivers with banks protected by groynes. *Journal of Hydraulic Research, IAHR, 33(2) 257-273.*
15. Rodi, W. (1984). *Turbulence models and their application in hydraulics: A State-of-the-Art Review.* IAHR Book Publication, Delft.
16. Przedwojski, B. (1997). Personal communication. *Department of Hydraulic Engineering, Agricultural University of Poznan, Poznan, Poland*
17. Ackers, P. & White, W. R. (1990). Sediment transport: the Ackers and White theory revised. Report No. SR 237, HR Wallingford, UK.
18. Van Rijn, L. C. (1993). *Principles of sediment transport in rivers, estuaries and coastal seas.* AQUA Publication, The Netherlands.
19. Koch, F. G. & Flokstra, C. (1981). Bed level computations for curved alluvial channels. *Proceedings, 19th Congress, IAHR, Subject A(d), New Dehli, India, (2) 357-364.*